



universität
wien

BACHELOR'S THESIS

INVESTIGATION OF BACKWARD VOLUME MAGNETOSTATIC SPIN WAVES USING PROPAGATING SPIN WAVE SPECTROSCOPY

submitted by
Fabian Majcen

in partial fulfilment of the requirements for the degree of
Bachelor of Science (BSc)

Vienna, 2022

Degree programme code: UA 033 676

Degree programme: Physics

Supervisor: Univ.-Prof. Dr. habil. Andrii Chumak

Contents

| | | |
|----------|--|-----------|
| 1 | Introduction | 4 |
| 2 | Theoretical background | 4 |
| 2.1 | Landau–Lifshitz–Gilbert equation (LLG) | 4 |
| 2.2 | Magnetostatic Spin Waves (MSW) | 5 |
| 2.2.1 | Backward Volume Magnetostatic Spin Waves (BVMSW) | 6 |
| 2.3 | Ferromagnetic resonance (FMR) | 8 |
| 2.4 | Biot–Savart law | 8 |
| 3 | Experimental setup, material and methods | 8 |
| 3.1 | Vector Network Analyzer (VNA) | 9 |
| 3.2 | Yttrium Iron Garnet (YIG) | 9 |
| 3.3 | Microstrip antennas | 10 |
| 4 | Experimental results | 13 |
| 4.1 | Sample thickness: 4.1 μm | 13 |
| 4.2 | Sample thickness: 7.78 μm | 16 |
| 4.3 | Sample thickness: 22.83 μm | 19 |
| 4.4 | Summary | 22 |
| 5 | Discussion | 24 |
| 5.1 | General | 24 |
| 5.2 | Signal strength | 24 |
| 5.3 | Bandwidth / Excitation efficiency | 25 |
| 6 | Conclusion | 27 |

Abstract

In the field of magnonics, named after magnons, the quanta of spin waves, the transmission, storage and processing of information using packets of spin waves is being studied [1]. In this thesis spin waves are investigated using propagating spin wave spectroscopy. The experiment shows, how sending an electrical signal through an antenna can excite spin waves inside a magnetic sample. On the same principle a signal is received back with a second antenna. This already demonstrates basic spin wave information transmission. Different spin wave properties are determined in this experiment. The frequency shift at different magnetic field strengths and the peak absorption at the ferromagnetic resonance frequency are shown. Furthermore, the influence of sample thickness on the spin wave signal is investigated and compared to the theory of magnetostatic spin waves. The excitation efficiency of the used antennas is calculated and compared with the measured signals. The correlation between the used antennas, the shape of signal and the broader frequency ranges for thicker samples is shown. Overall all of the experimental results fit well with the predictions of the theory.

1 Introduction

Spin waves are collective excitations of spins in magnetically ordered materials. They possess a diversity of dispersion characteristics. With the discovery of yttrium iron garnet (YIG), with its uniquely low magnetic damping, the interest in spin wave research spiked between 1960 and 1980. In this period a lot of analogue signal processing devices were developed. However, by now many have been replaced by new technologies. Nonetheless, recent years have seen a resurgence of interest in spin wave research, nowadays called 'magnonics'. In this field, named after magnons, the quanta of spin waves, the transmission, storage and processing of information using packets of spin waves is studied [1]. Using magnons, instead of electrons in electronics, as data carriers could bring many advantages. Since a magnon current does not involve motion of particles no Joule heating occurs. Furthermore, wave-based computing brings an additional degree of freedom and allows operations with vector variables. Even nanosized structural elements are possible, since spin wave wavelengths are only limited by the lattice constant of the magnetic materials [2].

In this thesis the propagation of backward volume magnetostatic spin waves (BVMSW) in magnetic thin films is investigated. Using propagating spin wave spectroscopy (PSWS), the characteristics of different sample thicknesses are compared at various magnetic field strengths. Micrometer-thick YIG samples are used as waveguides. Through data analysis the experimental ferromagnetic resonance frequency is determined and compared with theoretical predictions. First, after this introduction, in section 2 the necessary theoretical background is given. The motion of a magnetic moment in a magnetic field is described (Landau–Lifshitz–Gilbert equation) and built on to understand spin wave propagation. Then, in section 3, the experimental setup, the YIG samples and how spin wave excitation with microstrip antennas works is discussed. In section 4 the experimental results are presented individually for the different sample thicknesses and then briefly summarized. Following, in section 5, the results are discussed and compared to the theoretical predictions from section 2 and 3. Finally, in section 6, a general summary is given.

2 Theoretical background

2.1 Landau–Lifshitz–Gilbert equation (LLG)

The Landau–Lifshitz–Gilbert equation (LLG) describes the time evolution of a magnetic moment \vec{m} (or a magnetization \vec{M}) in an effective magnetic field \vec{H}_{eff} :

$$\frac{\partial \vec{m}}{\partial t} = -\gamma \vec{m} \times \vec{H}_{\text{eff}} + \alpha \vec{m} \times \frac{\partial \vec{m}}{\partial t} \quad (1)$$

With the reduced gyromagnetic ratio $\gamma = \mu_0 \gamma_e \approx 2.2128 \cdot 10^5 \text{ m A}^{-1} \text{ s}^{-1}$ and the Gilbert damping parameter α . If the magnetic moment and the magnetic field are not aligned, it

results in a precessional motion of the magnetic moment around the magnetic field axis. This is described by the first part of the equation ($\propto \vec{m} \times \vec{H}_{\text{eff}}$) and is portrayed in 1a. The second part of the equation ($\propto \vec{m} \times \frac{\partial \vec{m}}{\partial t}$) describes the damping of the precession. It can be seen in figure 1b and results in the alignment of the magnetic moment with the magnetization after some time. The magnetic moment considered here refers to magnetic moments inside a magnetic material. Therefore, physically, the energy lost in damping relates mainly to energy transferred to lattice vibrations. The combined motion results in a spiraling of the magnetic moment until it is aligned with the magnetic field (figure 1c) [3, 4].

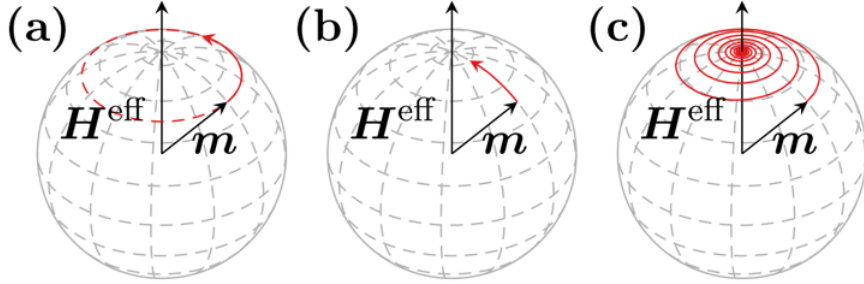


Figure 1: Motion of a magnetic moment \vec{m} inside a magnetic field \vec{H}_{eff} . Precessional (a) and dissipative (b) motion which results in the combined spiral (c) motion (taken from [4]).

2.2 Magnetostatic Spin Waves (MSW)

Spin waves are excitations in magnetic materials. In order for them to exist, the material needs to possess a magnetic order between neighboring spins, such as in ferro-, antiferro- or ferrimagnetic materials. If spins get disturbed and are no longer aligned with the magnetization, they start to precess in the way discussed in section 2.1 (equation 1 and figure 1). Through dipole-dipole and exchange interactions the precessing spins excite neighboring spin precession. This collective precession of spins which propagates through the material, is what is called a spin wave [3].

In the case of magnetostatic spin waves, the interaction between spins comes primarily from dipole-dipole interaction. They are often also called dipolar spin waves. The name 'magnetostatic' refers to the solutions to Maxwell's equations with a magnetostatic approximation. It assumes spin wave wavelengths significantly shorter than that of an electromagnetic wave of the same frequency and negligible displacement current. Exchange interaction is also neglected in this case. This holds true for big wavelengths since exchange interaction is highly sensitive to the relative orientation of neighboring spins. The typical wavelengths for MSW lie in the micrometer to millimeter range [1].

For MSW there are three different classes (modes) of spin waves. Magnetostatic surface spin waves (MSSW), forward volume magnetostatic spin waves (FVMSW) and backward

volume magnetostatic spin waves (BVMSW). They all have different dispersion characteristics. What distinguishes them from each other is their relative orientation between the propagation direction and the applied bias magnetic field which is used to magnetize the sample [1].

2.2.1 Backward Volume Magnetostatic Spin Waves (BVMSW)

For backward volume magnetostatic spin waves (BVMSW) the propagation direction, and thus the wavevector \vec{k} , is parallel to the magnetization. The propagation of BVMSW is through the whole volume of the material, although there are different thickness modes. Multiple of these modes can travel simultaneously at a given frequency [3]. However, only the lowest mode will be considered in this thesis.

Dispersion relation

The dispersion relation builds the connection between the wavenumber k and the frequency f of a wave. For BVMSW

$$f = \sqrt{f_H \left(f_H + f_M \frac{1 - e^{-kd}}{kd} \right)}, \quad (2)$$

$$\text{with } f_H = \frac{\gamma\mu_0 H_0}{2\pi} = \frac{\gamma B_0}{2\pi} \text{ and } f_M = \frac{\gamma\mu_0 M_{\text{eff}}}{2\pi}. \quad (3)$$

With the sample thickness d , the applied magnetic field H_0 (or the magnetic inductance B_0), the effective saturation magnetization M_{eff} , the magnetic permeability of free space μ_0 and the gyromagnetic ratio $\gamma = 1.76 \cdot 10^{11} \text{ rads}^{-1} \text{ T}^{-1}$ [1]. The effective saturation magnetization

$$M_{\text{eff}} = M_S - H_a \quad (4)$$

depends on the saturation magnetization M_S and the magnetocrystalline anisotropy field H_a . The magnetocrystalline anisotropy field is an intrinsic property of the material depending on its geometry which tends to orient the magnetization along certain crystal axis of symmetry [5]. For electron orbitals which are not spherically symmetric, the energy of the state depends on the orientation with respect to surrounding ions in the crystal. Because of spin-orbit coupling the energy of the net moment will then depend on its orientation with respect to the major axes of the crystal [3].

In YIG the iron ions in the ground state have no orbital angular momentum and therefore no spin-orbit coupling or magnetocrystalline anisotropy should occur. Nonetheless, experimentally a small anisotropy energy contribution can be found. The reason for this

is likely due to small spin–orbit interactions among the electronic substates neglected in the coupling scheme [3].

Similarly to the magnetocrystalline anisotropy, the shape anisotropy can lead to another contribution: the demagnetizing field. However, this is not considered here since the sample is thin and magnetized in plane [3].

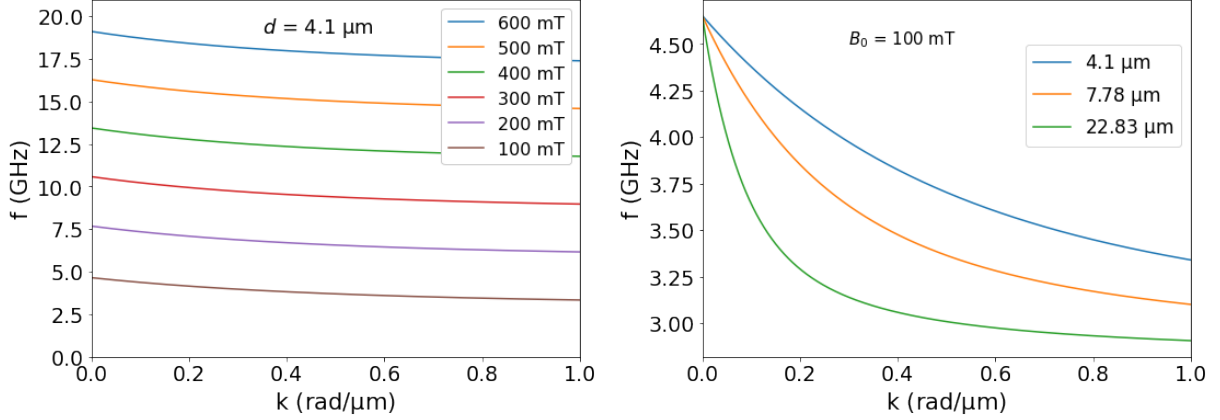


Figure 2: Dispersion relation (equation 2) for different magnetic fields (left) and different sample thicknesses (right). Calculated without consideration of the magnetocrystalline anisotropy field H_a with a saturation magnetization of YIG $M_S = 140 \text{ kA m}^{-1}$ [6].

In figure 2 the dispersion relation (equation 2) for different magnetic fields as well as different sample thicknesses can be seen. However, it was calculated without consideration of the magnetocrystalline anisotropy field H_a .

The phase velocity

$$v_P = \frac{\omega}{k} \quad (5)$$

is the ratio of the angular frequency $\omega = 2\pi f$ and the corresponding wave number k . The group velocity

$$v_G = \frac{\partial \omega}{\partial k} = -2\pi \cdot \frac{f_H f_M e^{-kd} \cdot (e^{kd} - kd - 1)}{2dk^2 \sqrt{f_H \left(f_H + f_M \frac{1 - e^{-kd}}{kd} \right)}} \quad (6)$$

corresponds to the slope of the dispersion curve. In the case of BVMSW the slope is negative which leads to different signs in phase and group velocities. This is the reason why BVMSW are called 'backward' waves. However, the information or energy is always carried by the group velocity [3].

2.3 Ferromagnetic resonance (FMR)

Ferromagnetic resonance (FMR) is the coupling between the magnetization of a medium and an electromagnetic wave which passes through it. The coupling leads to significant loss of power of the wave and is absorbed by the precessing magnetization. Here the precessing spins are all in phase with each other which is equivalent to a spin wave with infinite wavelength ($k \rightarrow 0$). The ferromagnetic resonance frequency (f_{FMR}) depends on the shape of the sample. In the case of a thin film with the field applied in plane the simplified Kittel formula

$$f_{\text{FMR}} = \frac{\gamma}{2\pi} \sqrt{B_0 (B_0 + \mu_0 M_{\text{eff}})} \quad (7)$$

can be used. It correlates to the point in the dispersion curve (figure 2) where $k = 0$ [5, 7].

2.4 Biot–Savart law

The Biot–Savart law describes the magnetic field created by a constant electric current I . A current-carrying conductor with the infinitesimal length element $d\vec{l}$ at \vec{r}' creates the magnetic induction

$$d\vec{B}(\vec{r}) = \frac{\mu_0}{4\pi} I d\vec{l} \times \frac{\vec{r} - \vec{r}'}{|\vec{r} - \vec{r}'|^3} \quad (8)$$

at the point \vec{r} [8].

3 Experimental setup, material and methods

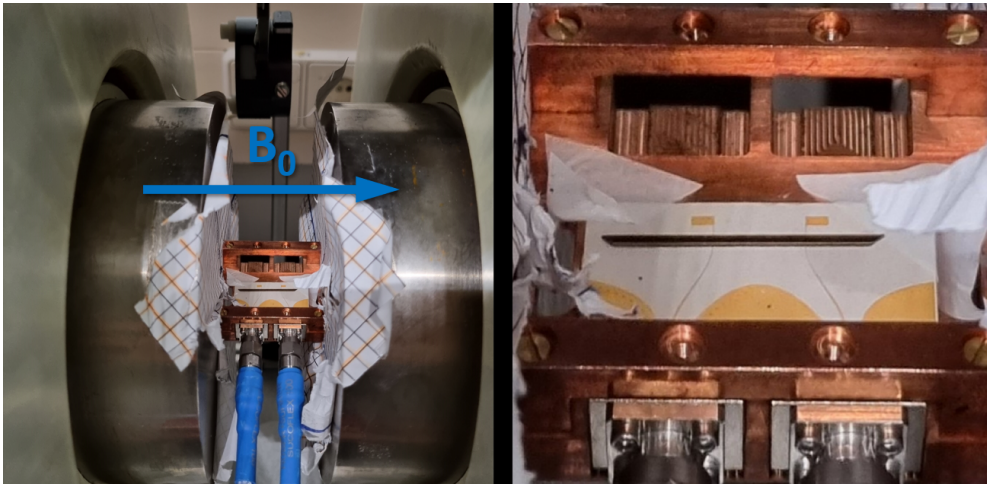


Figure 3: Experimental setup. Left: Sample holder inside the electromagnet. Right: Zoomed in view of the sample holder. Microstrip antennas and YIG sample can be seen.

The PSWS experimental setup (figure 3) consists of an electromagnet (controlled via a computer) including a Hall probe, a 2 port Vector Network Analyzer (VNA Anritsu MS4642B) and the sample holder with two microstrip antennas. As well as coaxial cables to connect the VNA to the sample holder.

A signal is sent from the VNA through the coaxial cables to one of the antennas. The current flowing through the antenna generates Oersted magnetic fields which excite spin waves inside the sample. The spin waves propagate along the waveguide and when near the second antenna induce a current inside of it. The distance between the antennas is 8 mm. This signal is received again by the VNA and compared to the input.

3.1 Vector Network Analyzer (VNA)

The VNA is rated for up to 20 GHz. It generates an AC microwave signal and also receives the signal again. When a signal is sent through port 1 with the amplitude a_1 part of the signal is reflected (b_1) and part of the signal is transmitted (b_2). The VNA shows this information through ratios of sent and received signal. These are called the S-parameters and are represented on a dB-scale. The reflection at Port 1

$$S_{11} = 20 \log_{10} \frac{b_1}{a_1} \quad (9)$$

and the transmission from Port 1 to Port 2

$$S_{21} = 20 \log_{10} \frac{b_2}{a_1}, \quad (10)$$

and analogous to these S_{12} and S_{22} when sending the signal from Port 2. To minimize the reflection at interfaces the impedance of the cables and the start of the antennas is matched to 50Ω . The VNA needs to be calibrated to the used cables with the desired number of data points. It calibrates the phase delay of the cables and ensures that the measurements of impedance are as accurate as possible. For the experiment a power of $0 \text{ dBm} = 1 \text{ mW}$ and averaging of 10 was used. Averaging reduces the effects of random noise on the measurement. The VNA conducts several measurements for each data point and displays the average values [9].

3.2 Yttrium Iron Garnet (YIG)

Thin film yttrium iron garnet (YIG) is used as samples. YIG is an insulating ferrimagnetic material and functions as a waveguide for spin waves. It stands out because of its extremely low magnetic damping (α from equation 1) which allows spin wave propagation over significant distances. The samples have a base of Gadolinium Gallium Garnet (GGG) which on both sides has the YIG crystal grown on. The exceptionally well matched lattice

constant of YIG and GGG allows the fabrication of high quality, defect-free unstressed films [1].

Microscopically YIG ($\text{Y}_3\text{Fe}_5\text{O}_{12}$) has a complex crystal structure. The five irons per formula are the only magnetic constituents. However, they are split in two magnetic sublattices orientated antiparallel to each other. Three iron in one and two in the other sublattice which results in a net magnetic moment due to one iron per formula unit [3]. The saturation magnetization of YIG at the temperature of 293 K is

$$M_S = 140 \text{ kA m}^{-1} [6].$$

The samples have trapezoidal ends (visible in figure 3) which cancel spin waves traveling into them minimizing reflection. For the experiment three different sample thicknesses were used. Thicknesses of $4.1 \mu\text{m}$, $7.78 \mu\text{m}$ and $22.83 \mu\text{m}$, with a width of 2 mm.

3.3 Microstrip antennas

In the PSWS setup the microstrip antennas excite spin waves via their generated magnetic fields. They consist of two electric conductors. Additionally to a small rectangular line they have a grounded plate. These two metallic parts are separated from each other by a dielectric insulator. This is the same principle as in coaxial cables. The electric and magnetic fields are guided inside of the dielectric between the conductors and are both mainly perpendicular to the direction of current. These kind of antennas/cables are necessary at microwave frequencies. For a normal wire the current would flow primarily on the surface of the material because of the skin effect [10].

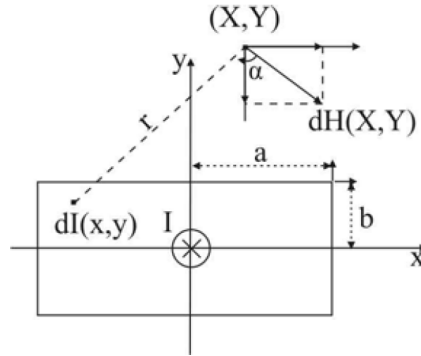


Figure 4: Coordinate system for calculation of the antenna field (taken from [11]).

The magnetic field of the antenna can be calculated by making a few assumptions. The high-frequency field is assumed to have the same strength as the static field at a given current density j and a homogeneous current distribution is assumed. A Cartesian coordinate system is used (figure 4) with conductor dimensions of $2a$ and $2b$. Only the field in the xy -plane will be considered, therefore the current is perpendicular to r which simplifies

the Biot-Savart law (equation 8) to [11]:

$$dH(X, Y) = \frac{I dx dy}{8\pi ab \sqrt{(x - X)^2 + (y - Y)^2}} \quad (11)$$

By integrating over the area of the antenna the x and y components of the magnetic field can be obtained (full derivation in [11]):

$$\begin{aligned} H_x(X, Y) = \frac{-I}{8\pi ab} & \left[(a - X) \left(\frac{1}{2} \ln \left(\frac{(b - Y)^2 + (a - X)^2}{(-b - Y)^2 + (a - X)^2} \right) + \frac{b - Y}{a - X} \arctan \left(\frac{a - X}{b - Y} \right) \right. \right. \\ & - \frac{-b - Y}{a - X} \arctan \left(\frac{a - X}{-b - Y} \right) \left. \right) - (-a - X) \left(\frac{1}{2} \ln \left(\frac{(b - Y)^2 + (-a - X)^2}{(-a - X)^2 + (-b - Y)^2} \right) \right. \\ & \left. \left. + \frac{b - Y}{-a - X} \arctan \left(\frac{-a - X}{b - Y} \right) - \frac{-b - Y}{-a - X} \arctan \left(\frac{-a - X}{-b - Y} \right) \right) \right] \quad (12) \end{aligned}$$

$$\begin{aligned} H_y(X, Y) = \frac{I}{8\pi ab} & \left[(b - Y) \left(\frac{1}{2} \ln \left(\frac{(b - Y)^2 + (a - X)^2}{(-a - X)^2 + (b - Y)^2} \right) + \frac{a - X}{b - Y} \arctan \left(\frac{b - Y}{a - X} \right) \right. \right. \\ & - \frac{-a - X}{b - Y} \arctan \left(\frac{b - Y}{-a - X} \right) \left. \right) - (-b - Y) \left(\frac{1}{2} \ln \left(\frac{(a - X)^2 + (-b - Y)^2}{(-a - X)^2 + (-b - Y)^2} \right) \right. \\ & \left. \left. + \frac{a - X}{-b - Y} \arctan \left(\frac{-b - Y}{a - X} \right) - \frac{-a - X}{-b - Y} \arctan \left(\frac{-b - Y}{-a - X} \right) \right) \right] \quad (13) \end{aligned}$$

The antenna used in the experiment has a width of 50 μm and a thickness of 15 μm therefore $a = 25 \mu\text{m}$ and $b = 7.5 \mu\text{m}$. For the current a simplified estimation can be made with the resistance of a conductor

$$R = \frac{\rho l}{A}, \quad (14)$$

with the antenna length of $l = 3 \text{ mm}$, the antenna cross-sectional area $A = 4ab$ and the resistivity of copper $\rho = 1.68 \cdot 10^{-8} \Omega\text{m}$. Furthermore, using the simple equation for electrical power

$$P = RI^2 = 1 \text{ mW}, \quad (15)$$

the current

$$I = \sqrt{\frac{P4ab}{\rho l}} = 122 \text{ mA}$$

can be calculated.

The magnetic field of this antenna, calculated with equations 12 and 13 is displayed on the left side of figure 5. On the right side of figure 5 $H_y(x, y = 8.5 \mu\text{m})$ is shown at a fixed y value close above the antenna (red dashed line on the left plot). For BVMSW the $H_y(x, y)$ component is what is relevant for spin wave excitation. $H_x(x, y)$ is parallel (or antiparallel) to the magnetization of the sample and therefore can not contribute to start spin precession. The antenna has different excitation efficiency depending on the

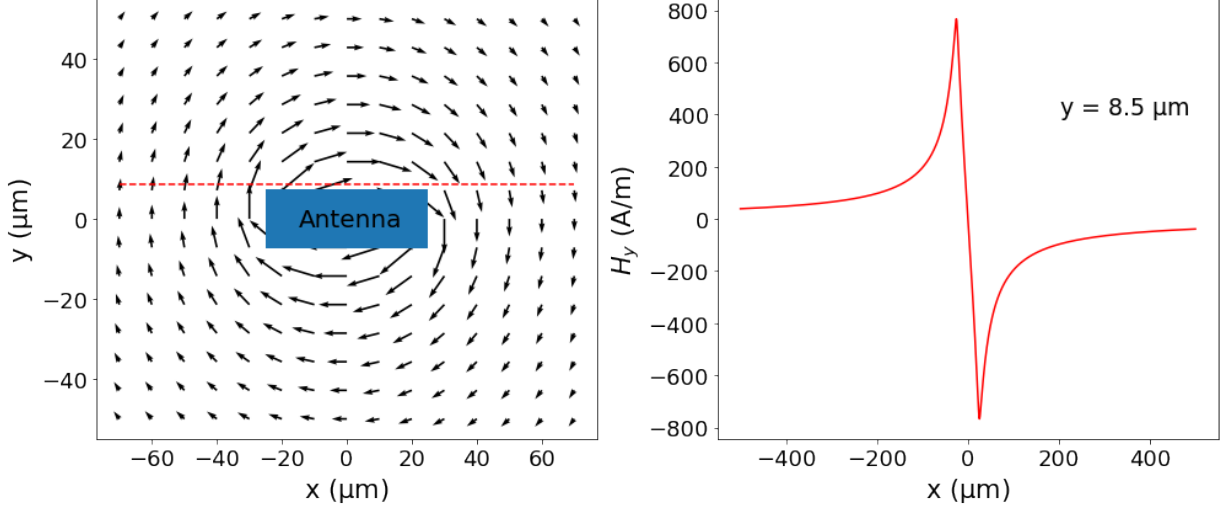


Figure 5: Magnetic field generated by the antenna on the left. $H_y(x, y)$ at $y = 8.5 \mu\text{m}$ (red dashed line on the left plot) on the right.

wavenumber k . The excitation efficiency is proportional to the Fourier transform of the relevant magnetic field component [10]:

$$\hat{H}_y(k_x) = \int_{-\infty}^{\infty} H_y(x, y) e^{ik_x x} \quad (16)$$

A normalized example of the Fourier transform is depicted in figure 6. Calculated at $y = 8.5 \mu\text{m}$ with integration limits of $\pm 0.5 \text{ mm}$.

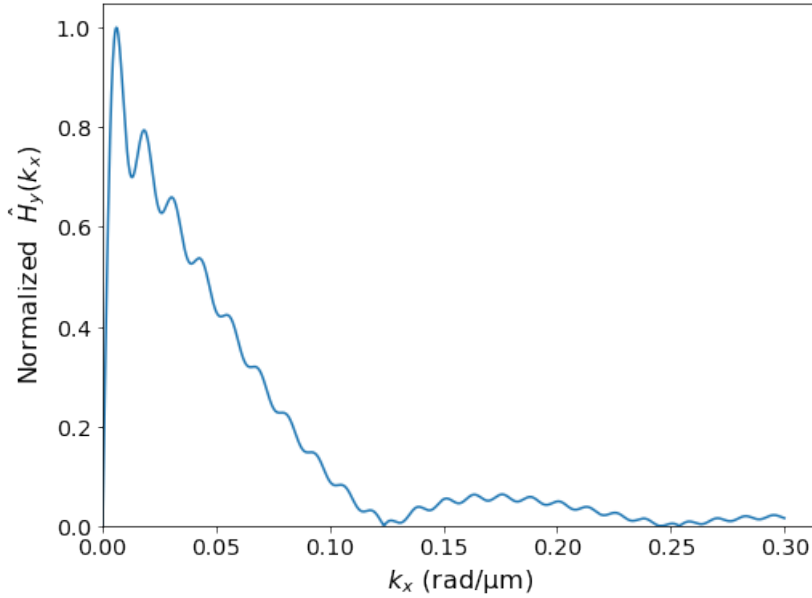


Figure 6: Normalized Fourier transform of $H_y(x, y)$ at $y = 8.5 \mu\text{m}$.

4 Experimental results

4.1 Sample thickness: 4.1 μm

The measured S_{21} signal of the BVMSW for the 4.1 μm thick sample is shown in figure 7 at different magnetic field strengths ranging from 100 mT to 600 mT.

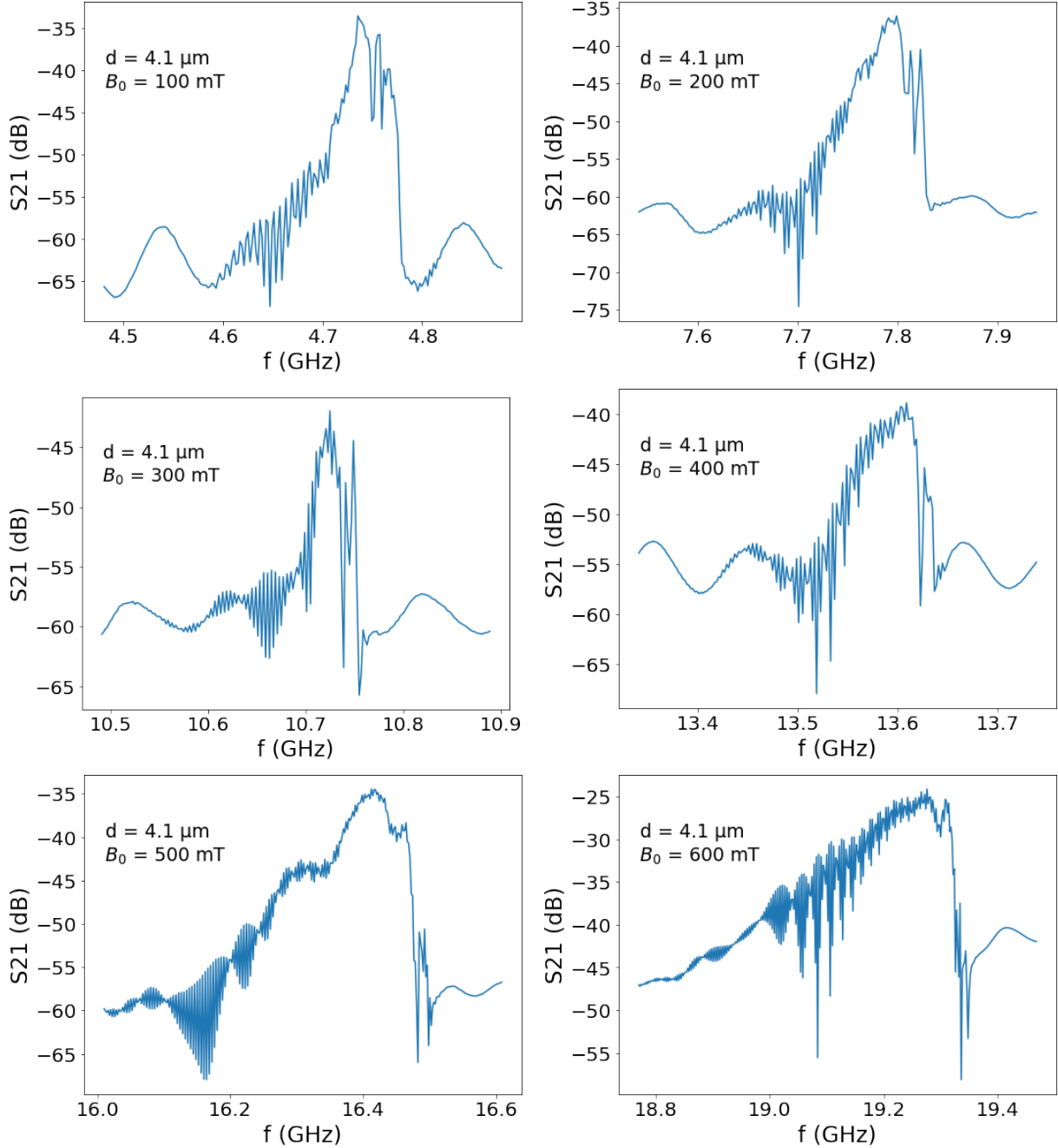


Figure 7: Spin wave signal for $d = 4.1 \mu\text{m}$ at different magnetic field strengths.

The f_{FMR} corresponds to the drop in intensity of the signal after the peak when looking at the signal from left to right. These experimental f_{FMR} values can be compared to the theoretical prediction from the dispersion relation (equation 2). First, only with consideration of the saturation magnetization instead of the effective saturation magnetization. An example is shown in figure 8 depicting BVMSW at 100 mT.

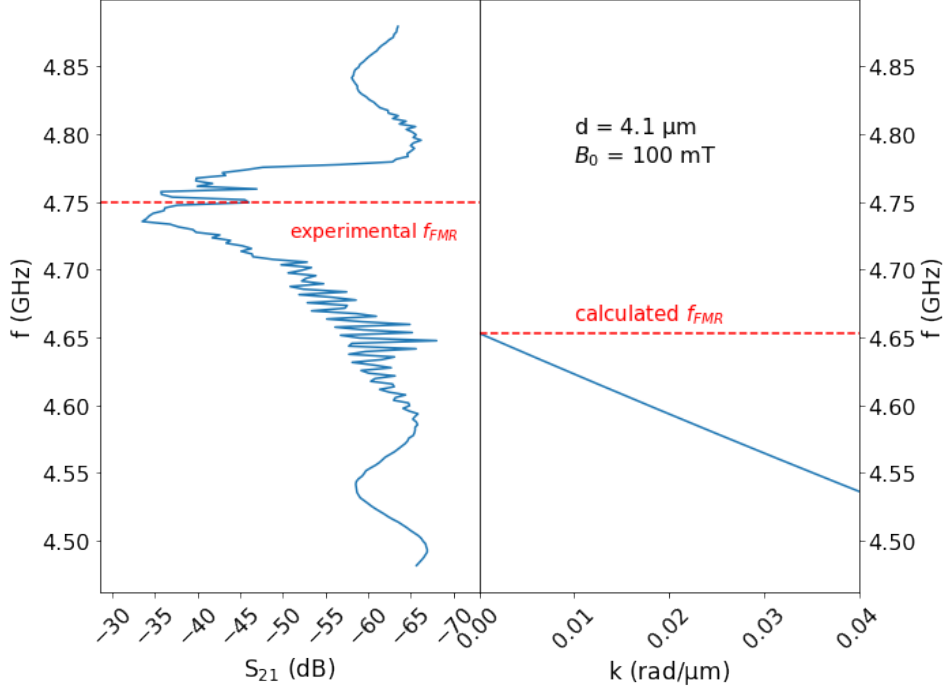


Figure 8: Comparison of analytical solution (without magnetocrystalline anisotropy field H_a) and experimental results. Spin wave signal of the 4.1 μm thick sample at 100 mT on the left. Dispersion relation from equation 2 on the right.

By matching the experimental and theoretical f_{FMR} values the magnetocrystalline anisotropy field H_a can be calculated. This can be done analytically with equation 2 by rewriting the equation for H_a at $f = f_{\text{FMR}}$ (experimental found f_{FMR}) and calculating the limit when k approaches zero:

$$H_a = M_S - \frac{2\pi}{\gamma\mu_0 f_H} (f_{\text{FMR}}^2 - f_H^2) \quad (17)$$

This is calculated for all measured magnetic field values. Again, the 100 mT signal is shown as an example in figure 9.

Finally, the Kittel formula (equation 7) can be used to calculate the f_{FMR} and compare the results with the experimentally obtained values. This is shown in figure 10 where the mean magnetocrystalline anisotropy field

$$\overline{H_a} = -11.12 \text{ kA m}^{-1}$$

from all measurements is used.

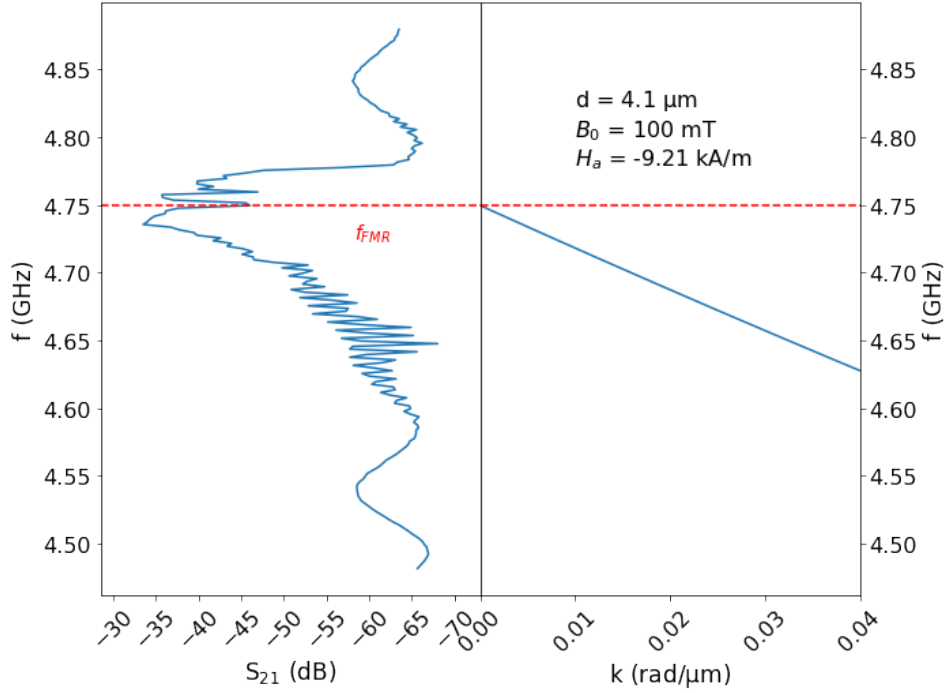


Figure 9: Matching of the f_{FMR} with the magneto-crystalline anisotropy field H_a from equation 17 for the $4.1 \mu\text{m}$ thick sample at 100 mT.

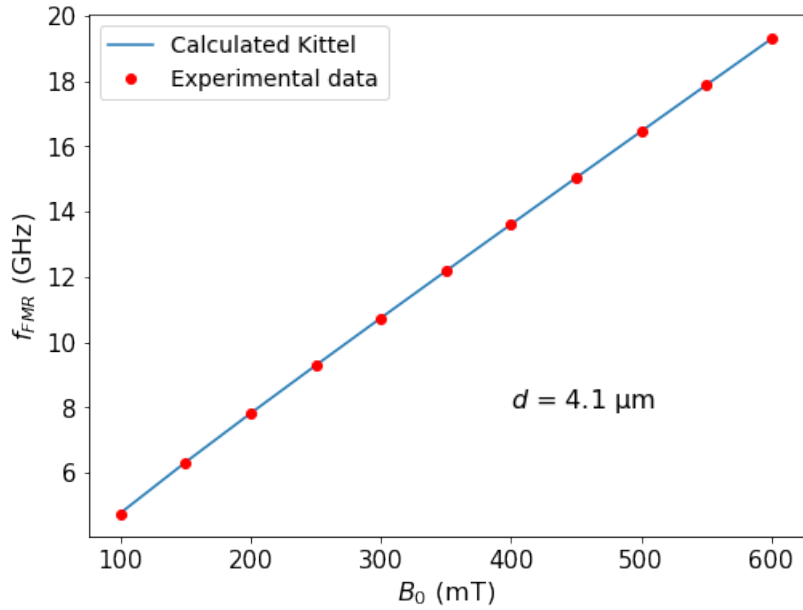


Figure 10: Comparison of the f_{FMR} calculated with Kittel formula (equation 7) using the mean magneto-crystalline anisotropy field $\overline{H_a}$ and the experimental found f_{FMR} for the $4.1 \mu\text{m}$ thick sample.

4.2 Sample thickness: 7.78 μm

The measured data from the 7.78 μm thick sample was evaluated identically as the 4.1 μm thick sample in section 4.1. First, the S_{21} signals are shown in figure 11.

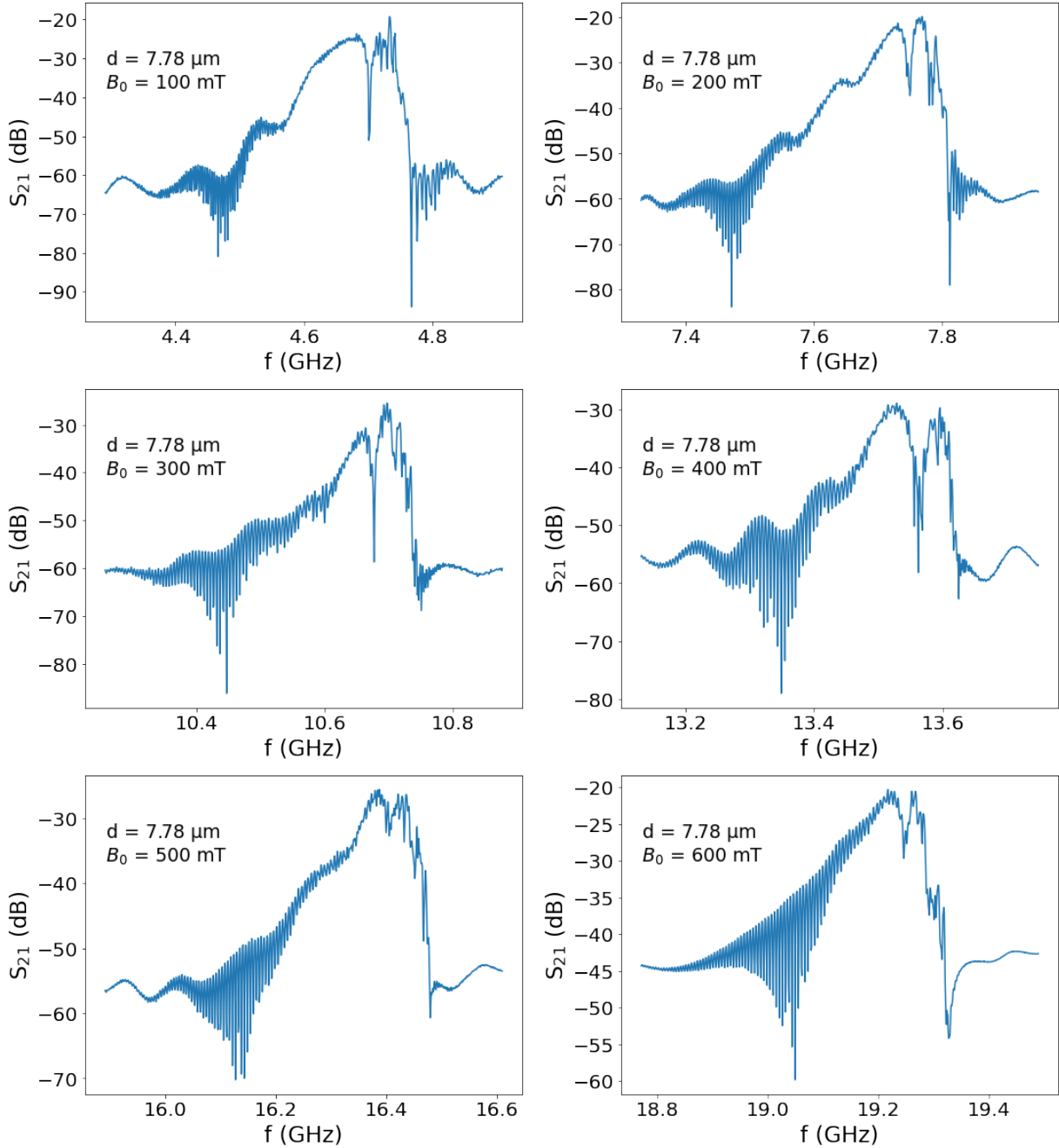


Figure 11: Spin wave signal for $d = 7.78 \mu\text{m}$ at different magnetic field strengths.

Then the FMR frequencies are compared to the theoretical prediction (equation 2) with an example shown in figure 12. Afterwards adjusted with the magnetocrystalline anisotropy field using equation 17 (figure 13).

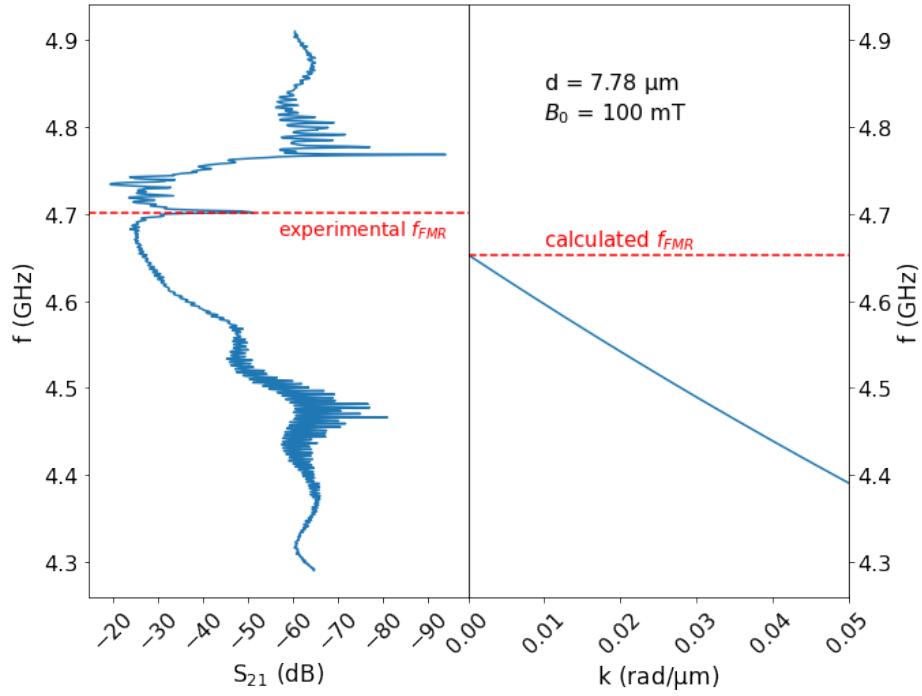


Figure 12: Comparison of analytical solution (without magnetocrystalline anisotropy field H_a) and experimental results. Spin wave signal of the $7.78 \mu\text{m}$ thick sample at 100 mT on the left. Dispersion relation from equation 2 on the right.

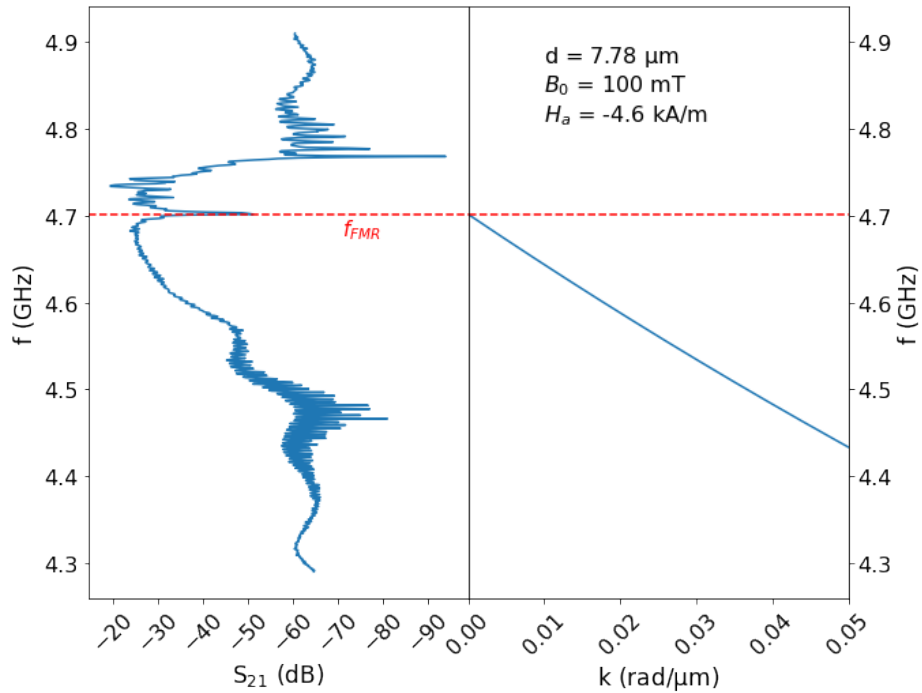


Figure 13: Matching of the f_{FMR} with the magnetocrystalline anisotropy field H_a from equation 17 for the $7.78 \mu\text{m}$ thick sample at 100 mT .

Finally, calculating the f_{FMR} with equation 7 using the mean magnetocrystalline anisotropy field

$$\overline{H_a} = -6.94 \text{ kA m}^{-1}$$

and comparing it with the experimental values (figure 14).

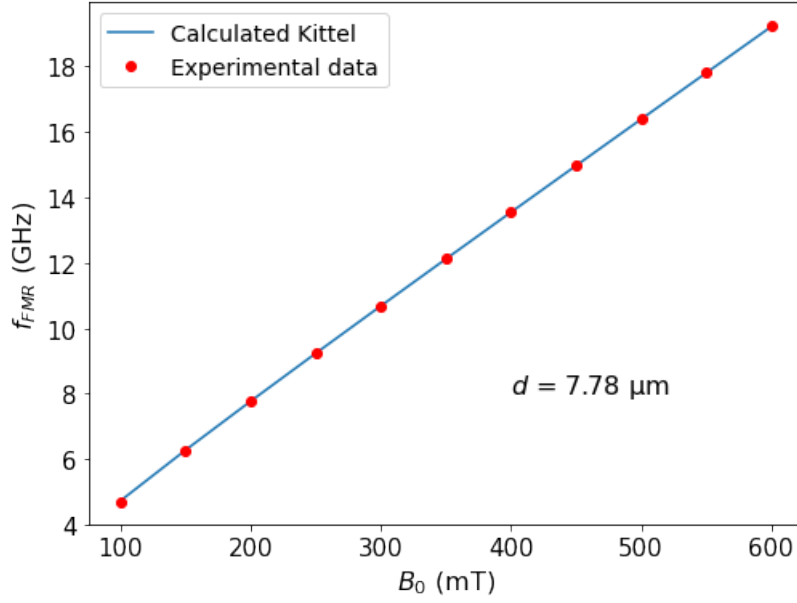


Figure 14: Comparison of the f_{FMR} calculated with Kittel formula (equation 7) using the mean magnetocrystalline anisotropy field $\overline{H_a}$ and the experimental found f_{FMR} for the $7.78 \mu\text{m}$ thick sample.

4.3 Sample thickness: 22.83 μm

The measured data from the 22.83 μm thick sample was evaluated identically as the 4.1 μm and 7.78 μm thick samples in sections 4.1/4.2. First, the S_{21} signals are shown in figure 15.

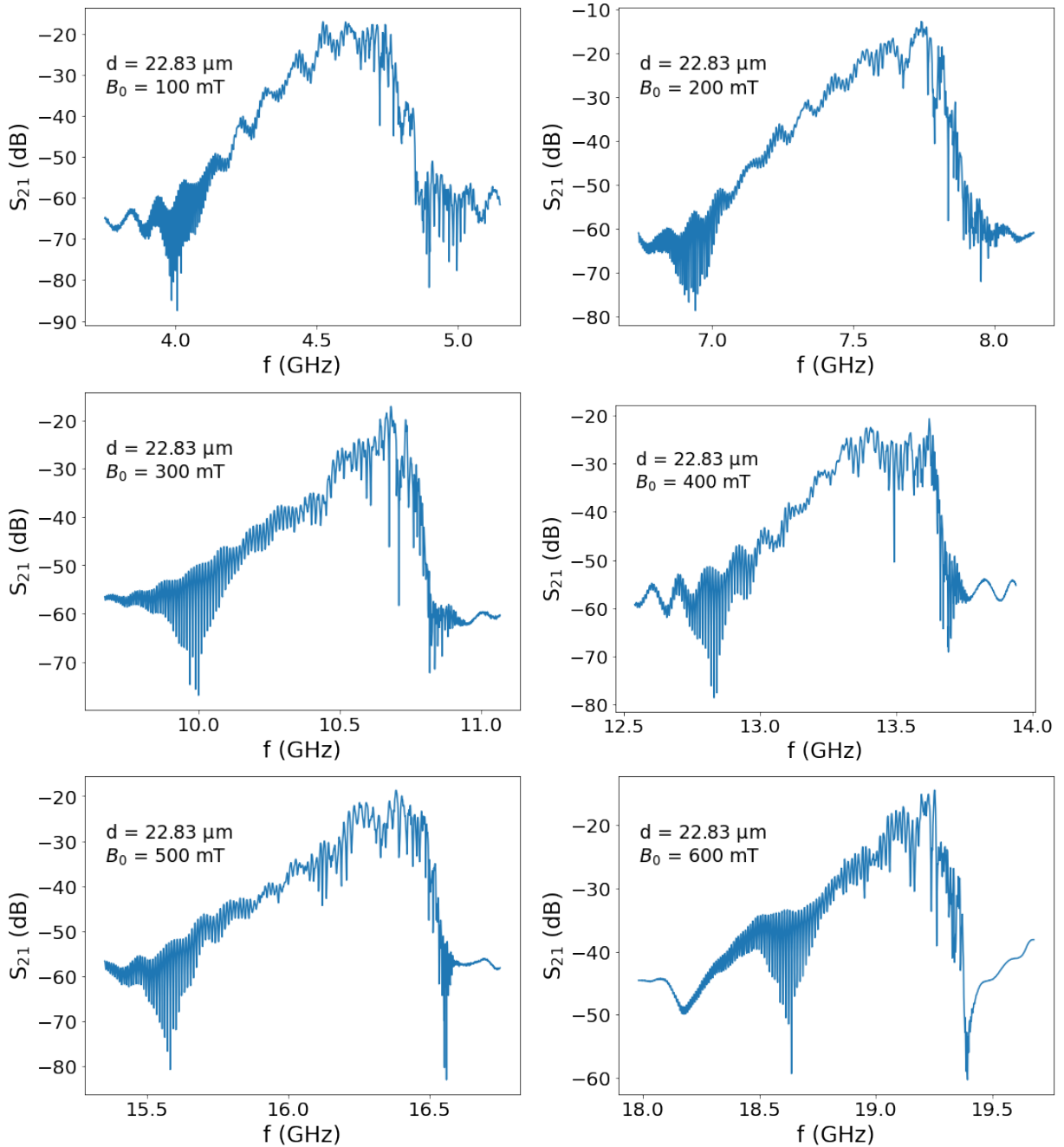


Figure 15: Spin wave signal for $d = 22.83 \mu\text{m}$ at different magnetic field strengths.

Then the FMR frequencies are compared to the theoretical prediction (equation 2) with an example shown in figure 16. Afterwards adjusted with the magnetocrystalline anisotropy

field using equation 17 (figure 17).

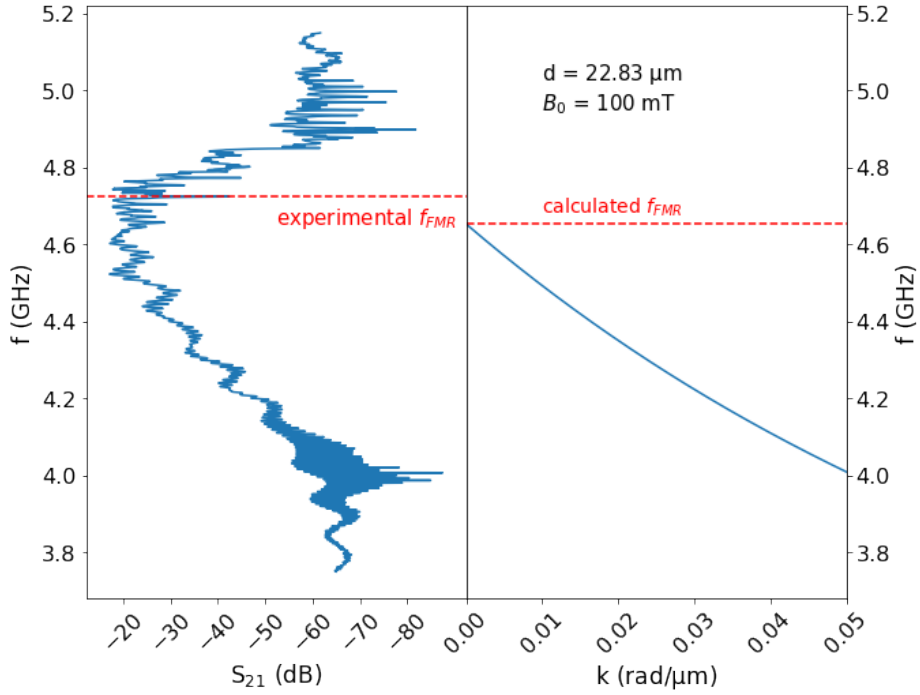


Figure 16: Comparison of analytical solution (without magnetocrystalline anisotropy field H_a) and experimental results. Spin wave signal of the 22.83 μm thick sample at 100 mT on the left. Dispersion relation from equation 2 on the right.

Finally, calculating the f_{FMR} with equation 7 using the mean magnetocrystalline anisotropy field

$$\overline{H_a} = -6.87 \text{ kA m}^{-1}$$

and comparing it with the experimental values (figure 18).

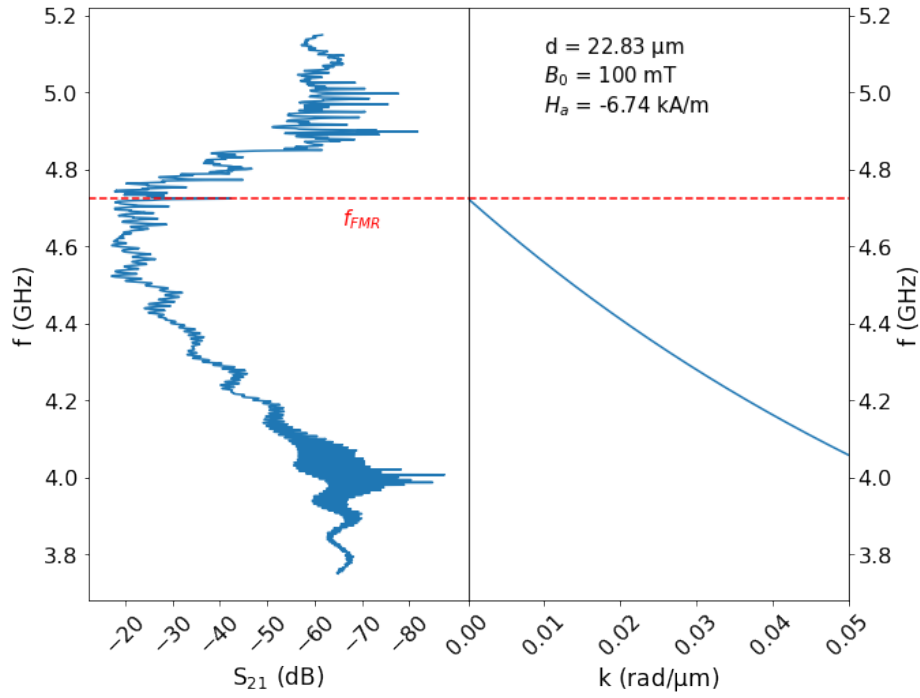


Figure 17: Matching of the f_{FMR} with the magneto-crystalline anisotropy field H_a from equation 17 for the 22.83 μm thick sample at 100 mT.

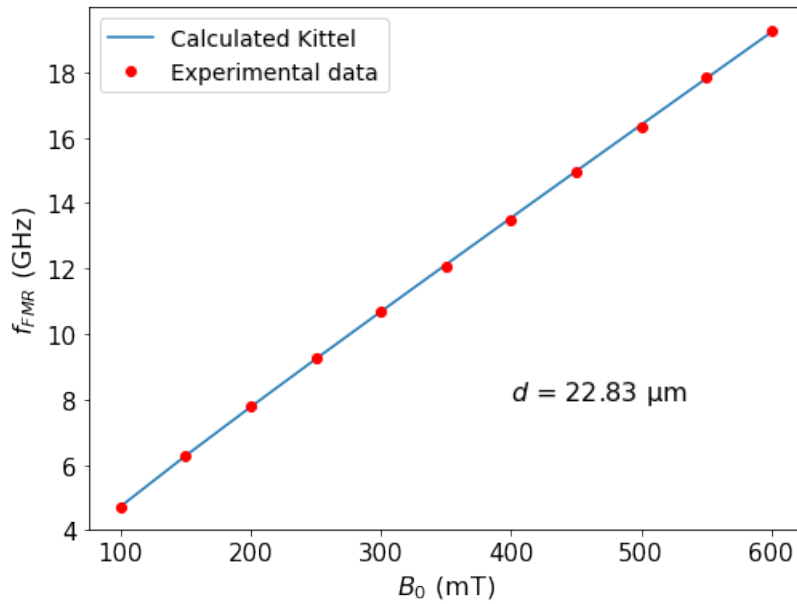


Figure 18: Comparison of the f_{FMR} calculated with Kittel formula (equation 7) using the mean magneto-crystalline anisotropy field $\overline{H_a}$ and the experimental found f_{FMR} for the 22.83 μm thick sample.

4.4 Summary

To compare the received signals of different sample thicknesses in the first picture of figure 19 a spin wave signal for the different thicknesses at the same magnetic field strength of 100 mT is shown. In the remaining pictures these signals are shown individually with their maximal signal strength $S_{21,\max}$ and their bandwidth at $S_{21,\max} - 15$ dB. For all of the measurements these values are summarized in table 1 and are additionally complemented with their respective mean values.

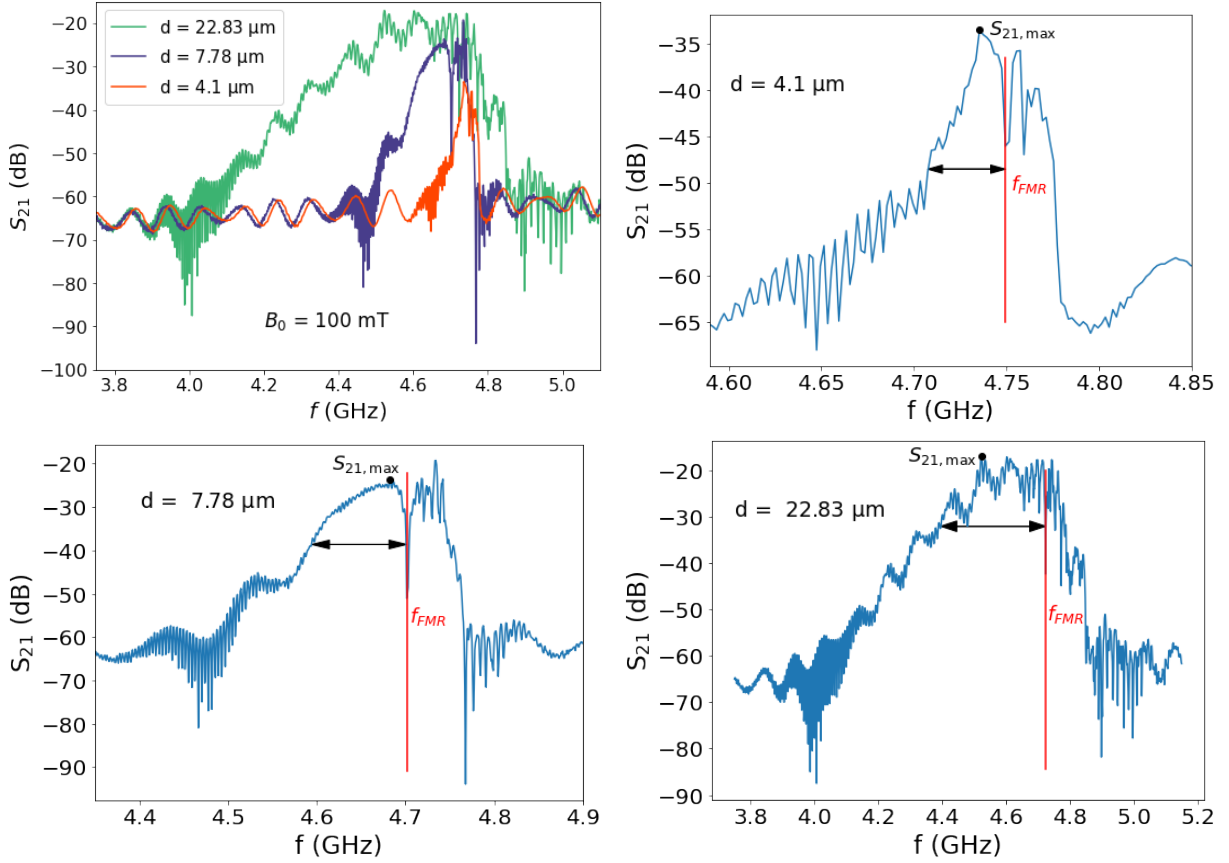


Figure 19: Comparison of spin waves signals of different sample thicknesses at the same magnetic field $B_0 = 100$ mT. First picture with all thicknesses together and followed by each one individually with their maximal signal strength $S_{21,\max}$ and their bandwidth at $S_{21,\max} - 15$ dB.

In table 2 all of the magnetocrystalline anisotropy fields from section 4.1 to 4.3 and their obtained mean values are summarized. Furthermore, the group velocities at all different fields and thicknesses were calculated with equation 6 at $k = 0.01$ rad/ μm .

Table 1: The maximal signal strength $S_{21,\max}$ and the bandwidth at $S_{21,\max} - 15$ dB for all different magnetic fields and sample thicknesses.

| | | $S_{21,\max}$ (dB) | | | Bandwidth (MHz) at $S_{21,\max} - 15$ dB | | |
|--------|---------------------|--------------------|--------|--------|---|--------|--------|
| | | 4.1 | 7.78 | 22.83 | 4.1 | 7.78 | 22.83 |
| B (mT) | d (μm) | | | | | | |
| 100 | | -33.52 | -23.66 | -17.10 | 42.00 | 107.15 | 327.85 |
| 150 | | -35.49 | -19.86 | -13.44 | 59.99 | 99.95 | 355.04 |
| 200 | | -36.07 | -21.33 | -12.77 | 71.99 | 122.34 | 360.63 |
| 250 | | -38.96 | -25.15 | -14.18 | 71.99 | 95.96 | 327.05 |
| 300 | | -41.97 | -30.67 | -17.17 | 51.99 | 104.75 | 249.49 |
| 350 | | -31.90 | -29.66 | -25.87 | 83.99 | 139.14 | 280.67 |
| 400 | | -38.90 | -28.94 | -22.52 | 95.99 | 132.74 | 317.45 |
| 450 | | -44.75 | -28.07 | -19.01 | 117.99 | 76.76 | 368.63 |
| 500 | | -34.44 | -25.56 | -21.44 | 199.98 | 157.53 | 262.28 |
| 550 | | -27.45 | -22.89 | -16.34 | 201.98 | 163.12 | 364.63 |
| 600 | | -24.15 | -20.32 | -14.45 | 233.98 | 171.92 | 427.00 |
| mean | | -35.24 | -25.10 | -17.66 | 111.99 | 124.67 | 330.97 |

Table 2: The magnetocrystalline anisotropy field H_a and the group velocity v_G at all different magnetic fields and sample thicknesses.

| | | H_a (kA/m) | | | v_G (km/s) at $k = 0.01$ rad/ μm | | |
|--------|---------------------|--------------|-------|-------|--|--------|---------|
| | | 4.1 | 7.78 | 22.83 | 4.1 | 7.78 | 22.83 |
| B (mT) | d (μm) | | | | | | |
| 100 | | -9.21 | -4.60 | -6.74 | -18.71 | -34.85 | -94.76 |
| 150 | | -9.79 | -5.11 | -8.03 | -21.07 | -39.2 | -106.19 |
| 200 | | -9.94 | -5.39 | -8.48 | -22.63 | -42.09 | -113.72 |
| 250 | | -10.65 | -5.87 | -8.69 | -23.76 | -44.16 | -119.08 |
| 300 | | -11.14 | -6.67 | -8.92 | -24.61 | -45.73 | -123.11 |
| 350 | | -11.84 | -7.79 | -2.57 | -25.28 | -46.95 | -126.25 |
| 400 | | -12.22 | -8.05 | -3.28 | -25.82 | -47.94 | -128.77 |
| 450 | | -12.69 | -8.19 | -6.84 | -26.26 | -48.75 | -130.84 |
| 500 | | -11.03 | -8.00 | -2.79 | -26.63 | -49.43 | -132.57 |
| 550 | | -11.59 | -8.06 | -9.54 | -26.95 | -50.01 | -134.03 |
| 600 | | -12.17 | -8.65 | -9.69 | -27.22 | -50.51 | -135.29 |
| mean | | -11.12 | -6.94 | -6.87 | | | |

5 Discussion

5.1 General

For all spin wave signals it was chosen to present S_{21} . In the case of BVMSW the propagation direction does not matter since they are 'volume' waves. Therefore, presenting S_{12} would have been equally valid. In figure 20 one example of S_{12} and S_{21} spin wave signal for $d = 4.1 \mu\text{m}$ at 100 mT is shown. Only small differences can be seen with the signal strength, the frequency range and the f_{FMR} point being essentially equivalent.

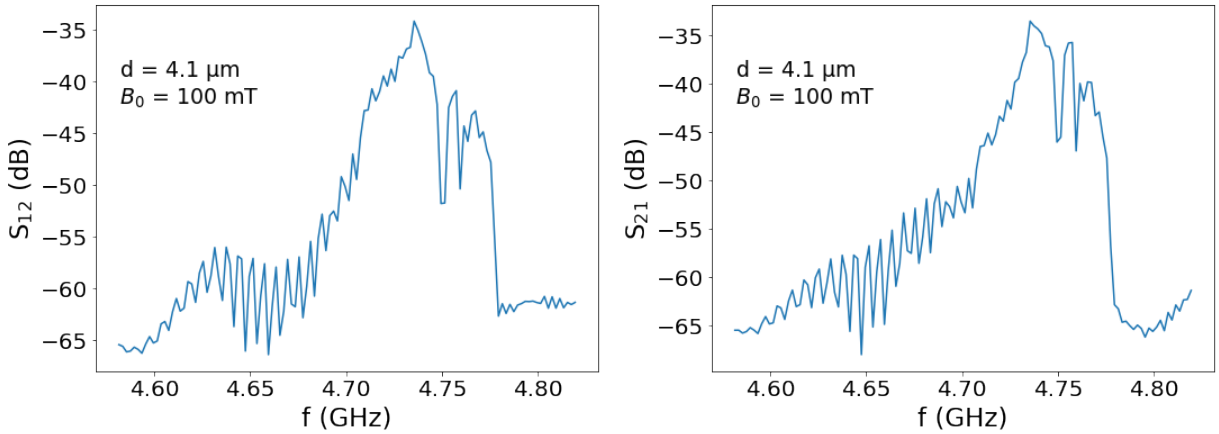


Figure 20: Comparison between S_{12} and S_{21} spin wave signal for $d = 4.1 \mu\text{m}$ at 100 mT.

In figure 7, 11 and 15 the correlation between frequency and applied magnetic field can be recognized. For bigger magnetic fields the spin wave signal shifts to higher frequencies. This matches with the theory of the dispersion relation (equation 2) as depicted in figure 2 where for stronger magnetic fields the frequency increases.

The comparison of the experimental evaluated f_{FMR} with the theoretical prediction from the Kittel formula (equation 7) in figure 10, 14 and 18 shows well matched data points. This gives certainty that the right f_{FMR} points were identified. However, PSWS is generally not that precise in this procedure and better methods can be used. With ferromagnetic resonance spectroscopy more accurate results could be achieved.

5.2 Signal strength

To compare signal strength, $S_{21,\text{max}}$ and the corresponding mean values were summarized in table 1. The data shows significantly stronger signals at higher sample thicknesses. The signal strength depends on the spin-wave propagation length. It scales with group velocity and the excitation efficiency of the antenna. The data in table 2 shows an increase in group velocity for thicker samples which therefore contributes to a stronger signal. In this

case the higher propagation speeds outweigh the damping of the spin wave. The second contribution comes from the excitation efficiency. In general the excitation efficiency scales with the volume of a magnetic material irradiated by the antenna field. Consequently, for thicker samples stronger signals are observed.

Analyzing the signal strength only frequencies smaller than the f_{FMR} were considered. Some of the signals had higher peaks at bigger frequencies, however these correspond to higher thickness modes (briefly mentioned in section 2.2.1) which are not considered.

5.3 Bandwidth / Excitation efficiency

In figure 7, 11 and 15 the shape of the spin wave signals can be analyzed. They peak shortly before the f_{FMR} point and then gradually fall off at lower frequencies. This is explained by the decrease in excitation efficiency of the antenna at increasing wavenumbers k . This was already calculated and shown (figure 6) in section 3.3. However, looking at the dispersion curve (figure 2) up to a specific (relatively low) k , because of a steeper slope it corresponds to a broader frequency range for the thicker samples. This change in the slope of the dispersion curve explains the larger bandwidth for thicker samples shown in figure 19 and displayed in table 1. These bandwidths were determined at $S_{21,\text{max}} - 15$ dB and only evaluated up to the f_{FMR} point. This is done as a generalized comparison of bandwidth between different thicknesses. The value of -15 dB was chosen to fit all of the experimental data since some of the signals of the $4.1 \mu\text{m}$ thick samples are only barely stronger than that. On the other hand, for the $22.83 \mu\text{m}$ thick sample the measured bandwidth was merely the top of the entire spin wave signal (see figure 19). Furthermore, there is some variation in signal shape which also influences the obtained bandwidths. The bandwidth increase from $4.1 \mu\text{m}$ to $7.78 \mu\text{m}$ in thickness is only barely recognizable. Comparing the mean values it increased from 111.99 MHz to 124.67 MHz. However, taking the $22.83 \mu\text{m}$ thick sample into consideration the increase in bandwidth becomes apparent without doubt with a mean bandwidth of 330.97 MHz.

To compare the excitation efficiency even better with the experimental spin wave signals the Fourier transform in dependence of the frequency instead of the wavenumber can be calculated. This is displayed in figure 21 using the $4.1 \mu\text{m}$ and $22.83 \mu\text{m}$ thick samples at 100 mT as an example. To transform from $\hat{H}_y(k_x)$ to $\hat{H}_y(f)$ the dispersion relation (equation 2) and the corresponding H_a from table 2 were used. Now the correlation between received signal and excitation efficiency can be recognized even more clearly. The matching f_{FMR} points and the decrease in signal strength/excitation efficiency can be seen. At about 40% of the maximal excitation efficiency the spin wave signals are no longer distinguishable from the base line transmission (at around -65 dB) which is always present due to leakage between the two antennas. Using the 40% as a reference the frequency ranges match well between the different signals and the excitation efficiency. A range of about 150 MHz for the thin and about 700 MHz for the thicker sample. Without considering higher thickness modes and looking at the whole recognizable signal.

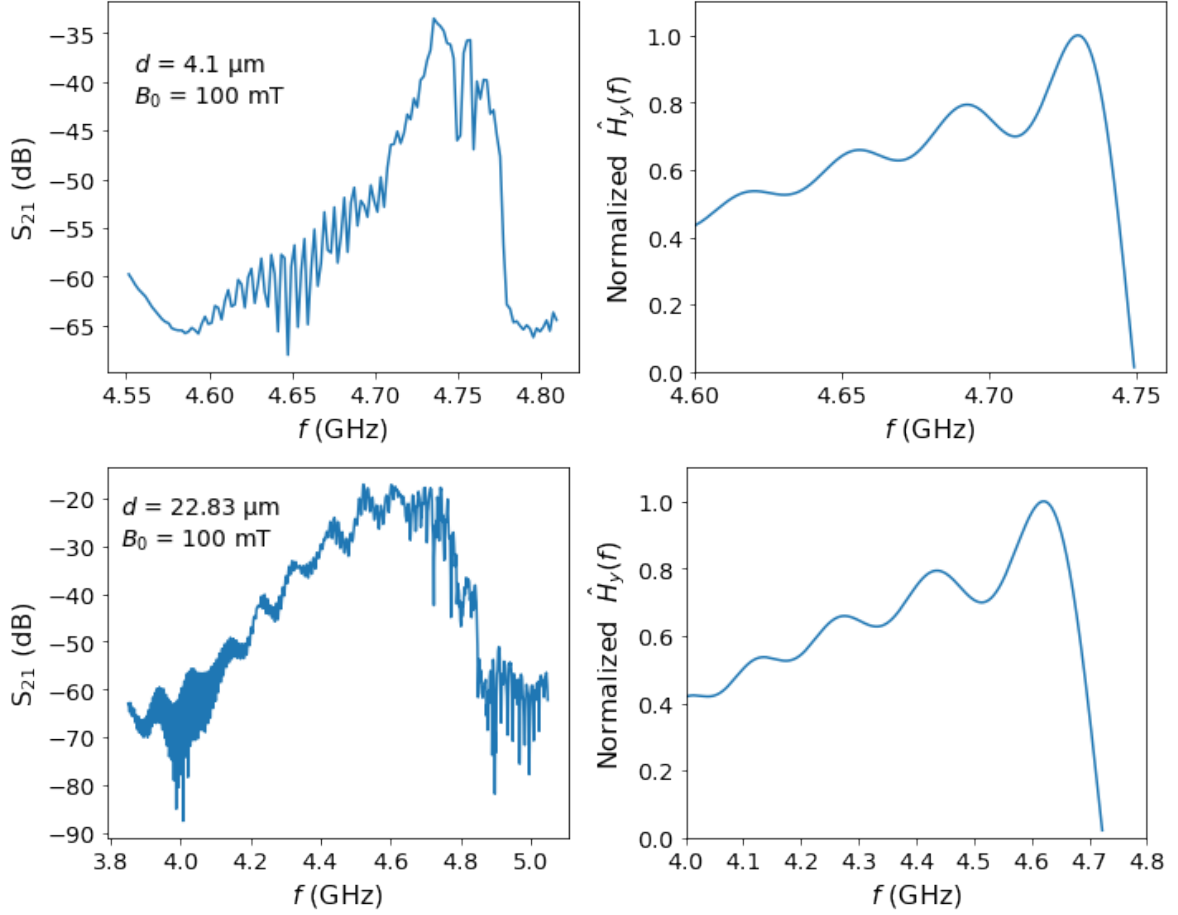


Figure 21: Comparison between a spin wave signal (left) and the calculated Fourier transform of the antennas magnetic field in dependence of the frequency (right).

When comparing the pictures in figure 21 it should be noted that the spin wave signal is on a dB-scale and the excitation efficiency is only proportional to the Fourier transform. It was also only calculated at one specific depth. Particularly at $y = 8.5 \mu\text{m}$ which is a depth of $1 \mu\text{m}$ under the surface of the sample and some simplifications were made in the calculation. When calculating the current a constant antenna width was assumed. This is actually not the case for the antenna used in the experiment. It is wider at the beginning where it is matched to an impedance of 50Ω and then gradually gets narrower until at its final width of $50 \mu\text{m}$. However, considering this in the calculation of the current makes it more complicated. Importantly, the normalized Fourier transform is the same. It is rather to give a sense of magnetic field strength of the antenna (figure 5). However, the reduction of the antenna width is important for the experiment. It improves excitation efficiency in the desired wavenumber regime. For comparison an antenna with double the width is considered in figure 22. The favorable excitation efficiency of the narrower antenna can clearly be recognized.

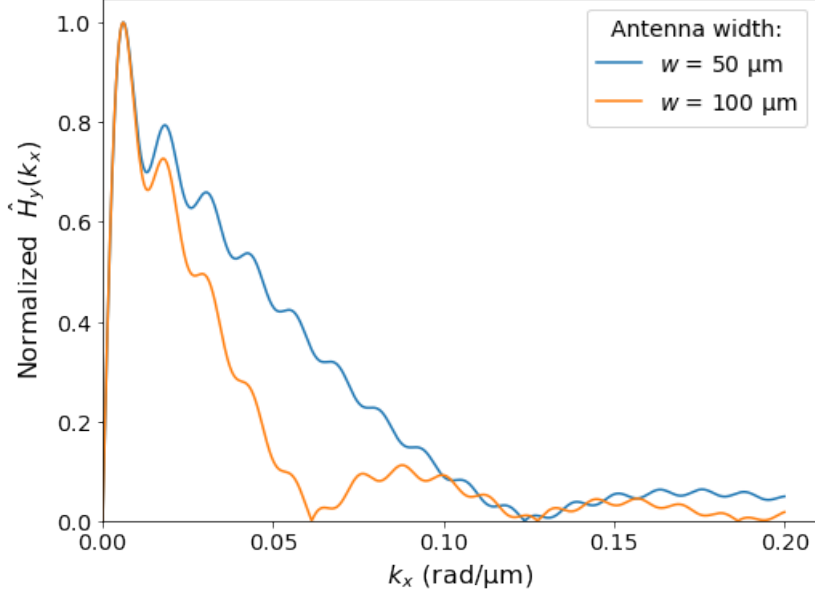


Figure 22: Normalized Fourier transform of $H_y(x, y)$ at $y = 8.5 \mu\text{m}$ for two different antenna widths.

6 Conclusion

In this thesis the propagation of BVMSWs in YIG waveguides was investigated. First and foremost the PSWS setup demonstrates how spin waves can be excited inside the sample and how a spin wave signal can be utilized to transfer information from one antenna to the other.

Different sample thicknesses of $4.1 \mu\text{m}$, $7.78 \mu\text{m}$ and $22.83 \mu\text{m}$ were studied at various magnetic field strengths ranging from 100 mT to 600 mT . The shift to higher frequencies at stronger magnetic fields was observed and matches with the theory of dispersion for BVMSW. The ferromagnetic resonance frequencies were determined by analyzing the experimental data. The magnetocrystalline anisotropy field was calculated by matching the data with the dispersion relation. Mean field strengths of -11.12 kA m^{-1} ($4.1 \mu\text{m}$), -6.94 kA m^{-1} ($7.78 \mu\text{m}$) and -6.87 kA m^{-1} ($22.83 \mu\text{m}$) were obtained. The experimental ferromagnetic resonance frequencies were compared to those calculated with the Kittel formula using the mean magnetocrystalline anisotropy field and are in accordance with each other. The combination of higher propagation speeds and bigger antenna irradiation volume in thicker samples results in increased signal strength for thicker samples. The comparison of signal strength mean values showed an increase from -35.24 dB ($4.1 \mu\text{m}$) to -25.10 dB ($7.78 \mu\text{m}$) and finally to -17.66 dB ($22.83 \mu\text{m}$). The magnetic field of the antennas which leads to the spin wave excitation was calculated and Fourier transformed to obtain information of excitation efficiency. The theoretical results match with the observed decrease in signal strength for lower frequencies and increase in bandwidth for higher thicknesses. Mean bandwidths of 111.99 MHz and 124.67 MHz were observed for the $4.1 \mu\text{m}$ and $7.78 \mu\text{m}$ samples respectively. However, the data showed a clear increase to 330.97 MHz for the $22.83 \mu\text{m}$ thick sample.

The influence of sample thickness on the received spin wave signal could be clearly identified. The main differences are all related to the variation in dispersion. The steeper slope for thicker samples results in a larger bandwidth and generally because of faster propagation speeds and bigger sample volume in stronger signals.

The PSWS experiment gives valuable introductory insight into the research of magnonics. Interesting spin wave properties are observed and the connection to the theoretical theory is established. For the measurements made all of the experimental gathered and analyzed data matches well with the theoretical predictions.

References

- [1] A. A. Serga, A. V. Chumak, and B. Hillebrands. Yig magnonics. *Journal of Physics D: Applied Physics*, 43, 2010.
- [2] Andrii V Chumak. Fundamentals of magnon-based computing.
- [3] Anil Prabhakar and Daniel D. Stancil. *Spin waves: Theory and applications*. Springer US, 2009.
- [4] Claas Abert. Micromagnetics and spintronics: Models and numerical methods. *European Physical Journal B*, 92, 6 2019.
- [5] Sergio M Rezende. Fundamentals of magnonics, 2020.
- [6] Kannan M Krishnan. Fundamentals and applications of magnetic materials.
- [7] Manuel Hohmann and Martin Von Den Driesch. Mikrowellenspektroskopie, 2005.
- [8] Siegmund Brandt, Hans Dieter Dahmen, Claus Grupen, and Tilo Stroh. Elektrodynamik - von den Maxwell-Gleichungen über die Elektro- und Magnetostatik zur elektromagnetischen Induktion, 2021.
- [9] Noise reduction techniques, https://na.support.keysight.com/pna/help/latest/S2_Opt/Trce_Noise.htm.
- [10] Dissertation Marc Vogel. Optisch induzierte Magnetisierungslandschaften zur Beeinflussung der Spinwellenpropagation.
- [11] Chumakov Dmytro. High frequency behaviour of magnetic thin film elements for microelectronics, 2006.